Exotic Reaction Front Migration and Stage Structure in Lithiated Silicon Nanowires

Lifen Wang,[†] Donghua Liu,[†] Shize Yang,[‡] Xuezeng Tian,[†] Guangyu Zhang,[†] Wenlong Wang,[†] Enge Wang,[‡] Zhi Xu,[†,*] and Xuedong Bai[†,§,*]

[†]Beijing National Laboratory for Condensed Matter Physics, Institute of Physics, Chinese Academy of Sciences, Beijing 100190, China, [‡]International Center for Quantum Materials, School of Physics, Peking University, Beijing 100871, China, and [§]Collaborative Innovation Center of Quantum Matter, Beijing 100190, China

ABSTRACT Nanostructured silicon anodes, which possess extremely high energy density and accommodate large strain without pulverization, have been developed rapidly for high-power lithium ion batteries. Here, using *in situ* transmission electron microscopy, the lithiation behavior of silicon nanowires with diameters smaller than 60 nm was investigated. The study demonstrated a direct dependence of the self-limiting lithiation on the pristine diameter. A "punch-through" lithiation process at the core of nanowires with pristine diameters slightly larger than the self-limiting threshold is suggested to occur with the consequent formation of a stage structure. Our work demonstrates the crucial role of mechanical stress and local defects in determining the migration and geometry of the reaction front at the mesoscopic scale. This intriguing finding holds critical significance for the application of silicon nanostructures in high-power lithium ion batteries.

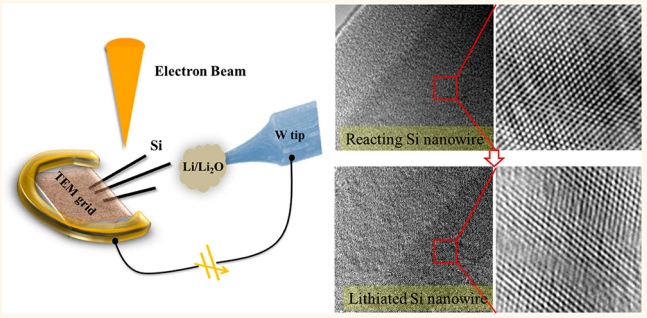

KEYWORDS: silicon nanowire · lithium ion battery · reaction front · stage structure · *in situ* transmission electron microscopy

Lithium ion batteries (LIBs) with improved capacity, rate, and cycle life are highly desired in the modern consumer electronics industry.[1−3] Nanostructured silicon is a very promising electrode material for high-performance LIBs because silicon has an extremely high theoretical gravimetric capacity at room temperature; additionally, the nanostructuring of silicon enhances mechanical fracture tolerance, resulting in increased cyclability.[4−10] Research on the lithiation mechanism and kinetics of silicon nanostructures is an emerging field.

The reaction front of lithiation is a critical interface that separates the lithiated phase from the pristine structure in LIBs. The electrochemical reaction that occurs at the interface is an essential process during battery operation, and the kinetics of the reaction front plays a decisive role in governing the rate performance of batteries.[11−14] Recently, studies on the lithiation kinetics in crystalline silicon nanostructures demonstrated that the orientation-dependent mobility of the reaction front led to highly anisotropic lithiation behavior.[15−18] The slowing of the reaction front upon lithiation, which ultimately gave rise to self-limiting lithiation behavior, was attributed to mechanical stress.[14,19] It is vital but rather difficult to understand all of the factors that can affect the reaction front, considering the complex local physical and chemical environment in Si nanostructures.[20−23] Here, we report the exotic behavior of reaction front migration and the formation of a novel stage structure in lithiated silicon nanowires. The results of this study demonstrate the crucial role of stress and local defects in determining lithiated/pristine interface migration.

RESULTS AND DISCUSSION

A nanoscale lithium ion half-cell with metallic lithium, lithia, and Si nanowire as the counter electrode, electrolyte, and working electrode, respectively, was constructed inside a JEOL 2010F transmission electron microscope (TEM) using a homemade double-tilt specimen holder with a

* Address correspondence to xuzhi@iphy.ac.cn, xdbai@iphy.ac.cn.

Received for review May 13, 2014 and accepted July 25, 2014.

Published online July 25, 2014
10.1021/nn502621k

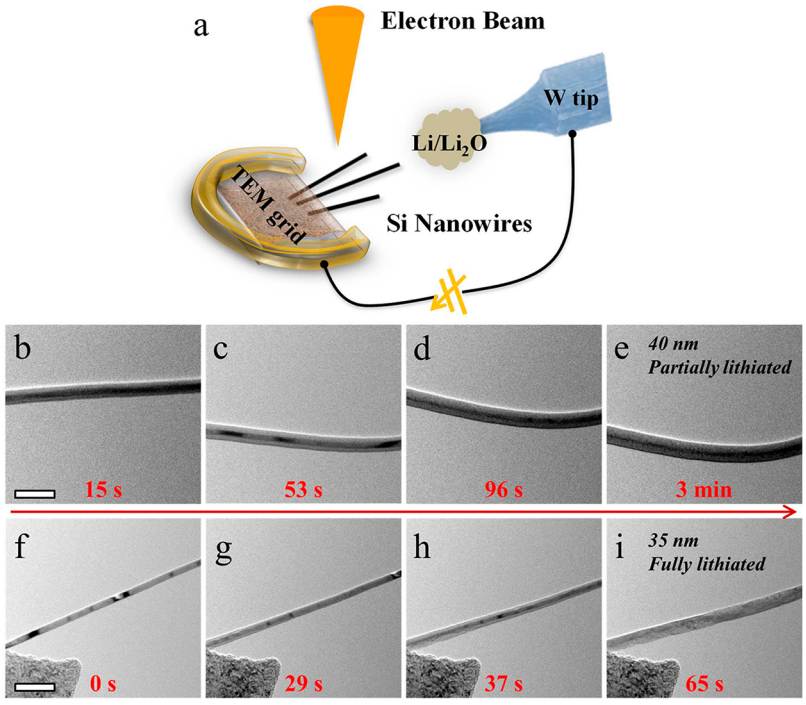

Figure 1. (a) Schematic of *in situ* TEM measurement setup. The CVD-grown Si nanowires on the substrates were scraped by a gold wire and further incorporated into the TEM grid. Once the selected nanowire contacted the lithium-loaded tungsten tip, which could be controlled by piezoelectric nanomanipulator, a lithiation voltage would be applied between the TEM grid and the tungsten tip, while the structural evolution during lithiation was investigated and recorded by the electron beam. (b−e) A series of bright-field TEM images of a Si nanowire with a pristine diameter of 40 nm during the first lithiation process. An amorphous Li_xSi shell was observed and grew progressively during lithiation. After 3 min, the core/shell structure was stable, indicating self-limited lithiation. (f−i) Images of another nanowire with a smaller diameter (35 nm) during the reaction process. After 65 s, the nanowire exhibited uniform contrast and was fully lithiated. Scale bar, 200 nm.

nanomanipulator.[24−27] The experimental configuration is schematically shown in Figure 1a. CVD-grown Si nanowires on the substrate were first attached to a gold wire and then incorporated into the TEM grid. The metallic lithium, which acted as a counter electrode, was scratched by an electrochemically etched tungsten tip in a glovebox. The oxide layer on the surface of the metallic lithium served as the solid electrolyte. The Li_2O-covered Li electrode was driven by a nanomanipulator, and once it contacted the free end of a selected nanowire, a potentiostatic hold of 3.5 V was applied across the two electrodes. Sequential TEM images of the first lithiation process for the nanowire with a diameter of 40 nm are shown in Figure 1b−e (see Supporting Information, Movie 1). Facilitated by the high contrast in electron transparency between the lithiated and pristine phases,[11,28,29] a distinct core/shell structure was observed. The lithiation of the Si nanowire was demonstrated to occur radially from the surface toward the inner bulk.[19] Upon lithiation, an amorphous Li_xSi (*a*-Li_xSi) shell with a gray contrast developed and grew, whereas the pristine, unreacted crystalline Si (*c*-Si) core shrank. The distinct contrast and the sharp boundary between the *a*-Li_xSi shell and *c*-Si core, regarded as the reaction front, indicated a two-phase mechanism of Li invasion into Si.[30,31] The lithiation became extremely slow as the core−shell interface moved deeply into the *c*-Si core. A relatively stable core/shell microstructure was obtained after 3 min, leaving the inner core unreacted. This self-limiting lithiation of the Si nanowires is consistent with previously reported experiments and is attributed to the stress-retardation effect, while high compressive stresses developed in the *a*-Li_xSi shell due to the large and abrupt change in Li concentration between two phases.[31−34]

In addition, we monitored another Si nanowire with a pristine diameter of 35 nm. Successive TEM images of the first lithiation process are shown in Figure 1f−i. Note that the contact between the Li_2O/Li and Si nanowire introduced strain along the nanowire; the asymmetrical dispersion of this strain gave rise to the initially striated contrast shown in Figure 1f. Upon lithiation, the nanowire swelled, and a core/shell structure with a gray contrast in the outer region gradually emerged (Figure 1g,h). This conventional core/shell microstructure surprisingly vanished, and a fully lithiated Si nanowire with uniform contrast was observed at 65 s, as shown in Figure 1i (see Supporting Information, Movie 2). This full lithiation behavior of the Si nanowire is in stark contrast to the self-limited lithiation behavior reported in previous studies.[17,19]

To examine the repeatability of this full-lithiation behavior, we carried out a series of comparative

experiments. Nine CVD-grown Si nanowires with pristine diameters smaller than 60 nm were selected systematically, and *in situ* characterizations were performed with the same setup at exactly the same lithiation voltage previously used. The final status of the first lithiation process is summarized in Figure 2 (see Supporting Information, Figures S1–S4). We can conclude that in our experiment, a nanowire with a diameter smaller than 38 nm could be fully lithiated, whereas an unreacted *c*-Si core remained when the pristine diameter was larger than such threshold.

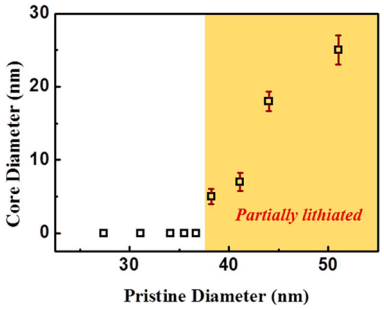

Figure 2. Diameter of the unreacted core in lithiated Si nanowire as a function of the pristine diameter. Final unreacted core diameters of nine Si nanowires with various pristine diameters demonstrated a size-dependent lithiation behavior.

Previously reported kinetics studies of Si nanowire lithiation focused mainly on the behavior of nanowires with the diameters larger than 100 nm.[17,19] The lithiation process was observed to be fast at the beginning and then apparently slowed down. This slowing of the reaction front was attributed to the stress that arises from Li concentration gradients across a reaction front.[14,30–32] The extremely slow velocity of the core–shell interface was noted as an indication of self-limiting lithiation after the thickness of the *a*-Li_xSi shell exceeded 100 nm, during which the stress accumulated to a tremendously high level and played a destructive role upon further lithiation.[19,34] In our experiment, for Si nanowires with a small pristine diameter (smaller than 38 nm), full lithiation could be achieved due to relatively low mechanical stress, which did not hinder the driving force for reaction.

Substantial effort was further devoted to studying the lithiation behavior of nanowires with diameters of ~38 nm. Figure 3a–c shows morphological images of one nanowire with a diameter of 38 nm during *in situ* lithiation, observed along the [111] zone axis. The large contrast between the amorphous, lithiated phase and pristine, crystalline pristine Si facilitated the observation of a radially propagating reaction front (Figure 3d–f). As shown in Figure 3f, the nanowire could not be fully lithiated, leaving a 13.8 nm-thick

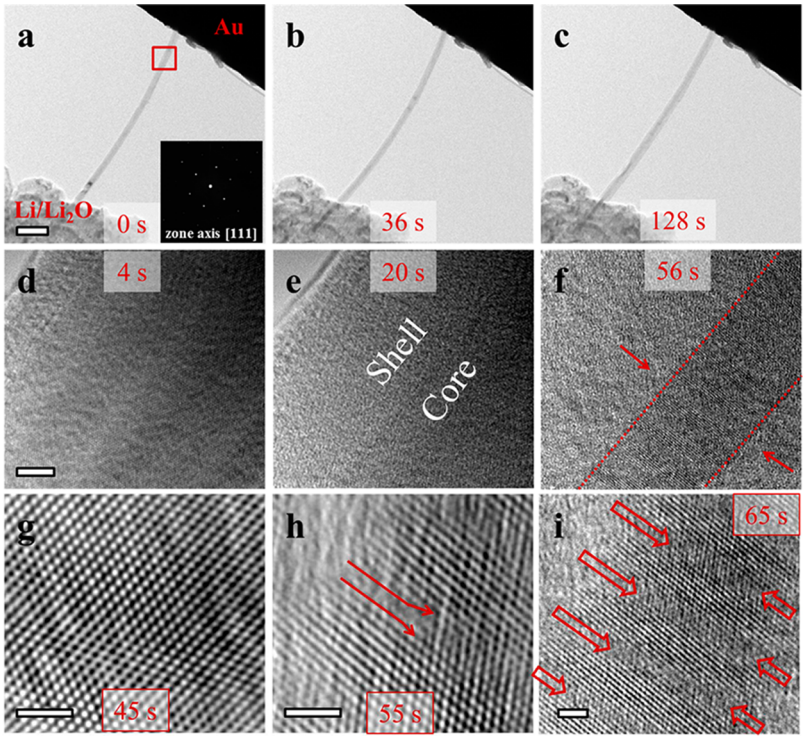

Figure 3. Stage structure of lithiated Si nanowire. (a–c) Consecutive low-resolution TEM images of a 38 nm diameter Si nanowire during the first lithiation process. The inset of (a) shows the selected area electron diffraction pattern of the nanowire. Scale bar, 200 nm. (d–f) The dynamic propagation of the shell–core interface. The red dashed lines highlight the reaction fronts. Scale bar, 5 nm. (g–i) High-resolution TEM images of the inner core during the lithiation process. The typical pristine Si structure is shown in (g). Upon further lithiation, a nanoscale lithiation path along the radial direction developed locally, as shown in (h). The red arrows indicate the lithiation path. An alternating sequence of lithiated and unlithiated, few atomic layer thick microstructures along the axial direction is shown in (i), revealing the formation of a stage structure in the core. Scale bar, 2 nm.

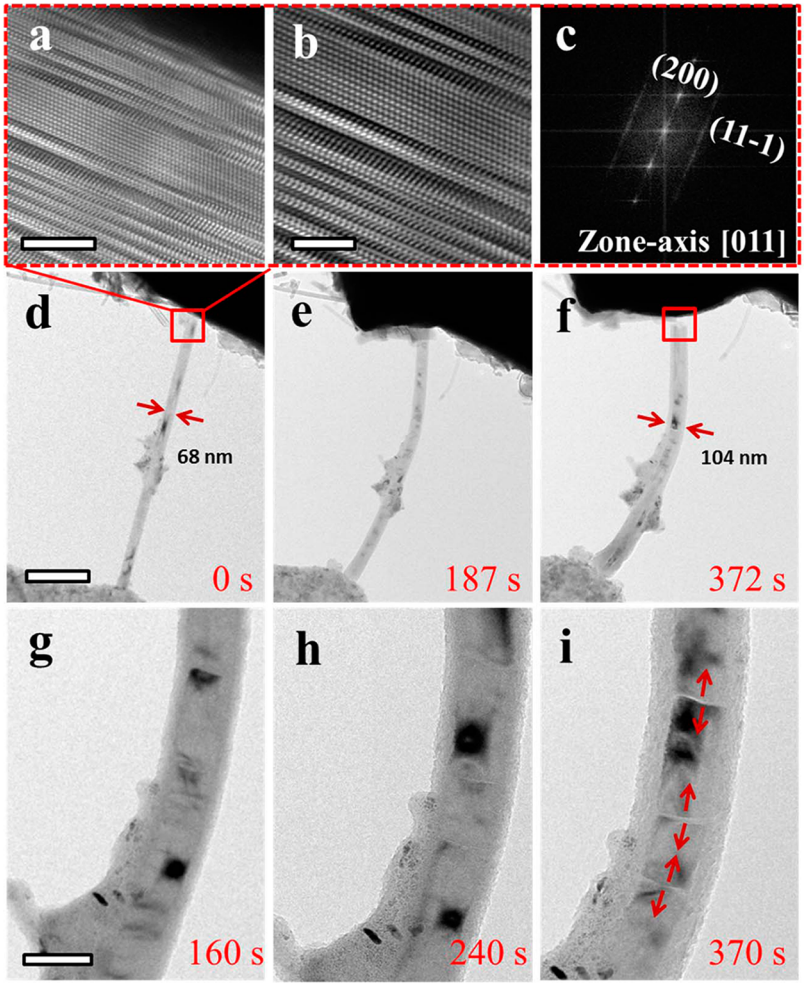

Figure 4. First lithiation process of a heavily doped silicon nanowire. (a–c) High-resolution TEM images and corresponding Fast Fourier Transform (FFT) data of the pristine nanowire. Linear defects along the radial direction are observed. Scale bar, 5 nm. (d–f) *In situ* TEM images of the first lithiation process of the nanowire. A lithiation induced crack is indicated by the red square in (f). Scale bar, 200 nm. (g–i) Consecutive TEM images of a selected area of the nanowire during lithiation. A bamboo-like, partially lithiated core is shown in (i).

unreacted core. A detailed understanding of the reaction front was gathered by monitoring the core at high resolution, as shown in Figure 3g–i. The pristine, unreacted core showed a representative lattice structure when observed along the [111] direction (Figure 3g). The entire shell–core interface barely moved toward the center of the nanowire after 45 s, whereas a local amorphous, lithiated phase appeared in the previously unreacted *c*-core. Figure 3h represents an intermediate stage of lithiation during which a newly formed lithiation channel along the radial direction partially passed through the core. During this stage, the mobility of the interface was locally enhanced such that the mesoscopic rise of the reaction front geometry along the radial direction could be observed. Finally, an alternating sequence of amorphous, lithiated Si and pristine, crystalline Si was observed along the axial direction, demonstrating a stage structure in the partially lithiated core. Amorphous lithiated phase (~2 nm) was interbedded with the pristine phase in an orderly manner (see Supporting Information, Figures S5 and S6). After the development of an amorphous-shell/stage-structure-core, the microstructure of the Si nanowires did not alter, even with prolonged lithiation.

Lithiation dominated by a ledge mechanism in Si nanowires was reported previously, and the origin of the orientation-dependent mobility of the reaction front was comprehensively studied.[15,17,35,36] The amorphous Li_xSi shell was observed to have been produced through the layer by layer peeling off the atomic facets. It should be noted that the diameters of the Si nanowires investigated in those studies were larger than 100 nm, with the *c*-core larger than 50 nm after self-limiting lithiation. In the present study, when the pristine size of Si nanowires fell within the most suitable range (38–40 nm here), the smooth, lithiated/unlithiated interface shrank into several ~2 nm wide subinterfaces with relatively uniform spacing (~3 nm), This exotic migration of the reaction front led to the punch-through

of a series of nanoscale radial lithiation channels and then created stage structures in the core. Our results indicate that the parameters governing this vertical punch-through mechanism are the diameter of each pristine nanowire and that of the final core structure. It is speculated that the stress accumulated in this system (pristine diameter of 38 nm and final core diameter of 13.8 nm) is sufficient to hinder full lithiation. However, it is not sufficiently high to completely prevent the migration of the lithiation interface. As a result, a partially lithiated core was observed. This well-ordered lithiation pattern in the partially lithiated core is analogous to the staging phenomenon observed in graphite intercalation compounds, in which a strain mechanism is suggested to give rise to the stage structure.[37] In the system considered in this study, the lattice-stress interactions are long-range, and the resulting stress energy must be shared by all atomic layers of the silicon phase. To achieve the minimum stress energy, the Li–Si alloy phase is packed in the pristine structure with a well-ordered distribution.

The stage structure observed in the partially lithiated core of a nanowire clearly demonstrates that the stress induced by lithiation can alter the local geometry of the reaction front at the mesoscopic scale. To shed light on the role of the local environment on the migration of the lithiation interface, we further carried on an *in situ* experiment on heavily doped Si nanowires with radial linear defects (Supporting Information Figure S7), which facilitated the creation of new lithiation paths. Figure 4a–c shows a CVD-grown, heavily doped Si nanowire with a pristine diameter of 68 nm and a high density of linear defects along the (110) atomic lattice plane. Upon lithiation, the nanowire swelled to 104 nm in diameter and fractured into two segments (indicated by the red square in Figure 4f). The *in situ* TEM images in Figure 4g–i show that an amorphous shell developed with the elongation and swelling of the wire (see Supporting Information, Movie 3). A bamboo-like structure with three gray knots appeared in the core, as shown in Figure 4i. The pristine, undoped Si nanowire with a diameter of 68 nm would follow self-limiting lithiation behavior, showing a clear core–shell structure with a flat interface. However, for heavily doped Si, the interface mobility was locally enhanced by radial defects (see Supporting Information, Movie 4). In other words, the existence of radial linear defects weakened the Si–Si covalent bonding and thus assisted in the creation of new ion transport paths along the radial direction. As a result, nanoscale lithiation channels penetrated the unreacted crystalline core, resulting in a bamboo like, partially lithiated core.

CONCLUSIONS

In conclusion, *in situ* TEM lithiation characterizations of Si nanowires with diameters smaller than 60 nm have been presented. It was observed that the self-limiting lithiation of the Si nanowires showed size dependence behavior and Si nanowires with diameters smaller than 38 nm could be fully lithiated. We found that the geometry and migration of the lithiation interface can be altered and enhanced by an environment characterized by local stress and defects at the mesoscopic scale, leading to a novel stage structure in the crystalline core. The observed size-dependent lithiation behavior holds implications for achieving high charge capacity in lithium ion batteries. Additionally, our work represents an important advancement in the fundamental understanding of the lithiation mechanism of silicon for promoting the application of Si nanowires in high-energy-density lithium ion batteries.

METHODS

Si nanowires were synthesized *via* the vapor–liquid–solid growth technique. Growth was carried out at 450 °C for intrinsic nanowires and 470 °C for n-type nanowires under a pressure of 8.5 and 9 Torr, respectively, by CVD. Gold colloidal nanoparticles with diameters of ~40 nm were spin-coated on a thermally oxidized SiO_2 layer (300 nm in thickness) on a Si (p^{+2}) substrate as the growth catalyst. High-purity silane carried by hydrogen was used as the precursor, and phosphine (1000 ppm in H_2 carrier) served as the n-doping gases.

In situ characterization was carried out using a homemade TEM-SPM specimen holder with a nanomanipulator in a JEOL2010F TEM at 200 kV. Si nanowires were attached to a gold wire and then loaded onto the specimen holder. Metal lithium was scratched by an electrochemically etched tungsten tip. A homemade piezo-driven nanomanipulator was used to manipulate the tungsten tip to contact a selected nanowire inside the column. Electrochemical measurements were conducted using Agilent B2912A under the potentiostatic mode.

Conflict of Interest: The authors declare no competing financial interest.

Supporting Information Available: Procedures and additional data. This material is available free of charge *via* the Internet at http://pubs.acs.org.

Acknowledgment. We acknowledge financial support from National 973 program (Grant Nos. 2012CB933003 and 2013CB93201), Natural Science Foundation (Grant Nos. 11004230, 51172273, 21322304 and 11290161), and the Strategic Priority Research Program B of the Chinese Academy of Sciences (Grant No. XDB07030100) of China.

REFERENCES AND NOTES

1. Dunn, B.; Kamath, H.; Tarascon, J. M. Electrical Energy Storage for The Grid: A Battery of Choices. *Science* **2011**, *334*, 928–935.
2. Tarascon, J. M. Key Challenges in Future Li-Battery Research. *Philos. Trans. R. Soc., A* **2010**, *368*, 3227–3241.
3. Tarascon, J. M.; Armand, M. Issues and Challenges Facing Rechargeable Lithium Batteries. *Nature* **2001**, *414*, 359–367.
4. Li, H.; Huang, X. J.; Chen, L. Q.; Wu, Z. G.; Liang, Y. A High Capacity Nano-Si Composite Anode Material for Lithium Rechargeable Batteries. *Electrochem. Solid St.* **1999**, *2*, 547–549.
5. Chan, C. K.; Peng, H. L.; Liu, G.; McIlwrath, K.; Zhang, X. F.; Huggins, R. A.; Cui, Y. High-Performance Lithium Battery Anodes Using Silicon Nanowires. *Nat. Nanotechnol.* **2008**, *3*, 31–35.

6. Kasavajjula, U.; Wang, C. S.; Appleby, A. J. Nano- and Bulk-Silicon-Based Insertion Anodes for Lithium-Ion Secondary Cells. *J. Power Sources* **2007**, *163*, 1003–1039.
7. Arico, A. S.; Bruce, P.; Scrosati, B.; Tarascon, J. M.; Van Schalkwijk, W. Nanostructured Materials for Advanced Energy Conversion and Storage Devices. *Nat. Mater.* **2005**, *4*, 366–377.
8. Park, M. H.; Kim, M. G.; Joo, J.; Kim, K.; Kim, J.; Ahn, S.; Cui, Y.; Cho, J. Silicon Nanotube Battery Anodes. *Nano Lett.* **2009**, *9*, 3844–3847.
9. Key, B.; Morcrette, M.; Tarascon, J. M.; Grey, C. P. Pair Distribution Function Analysis and Solid State NMR Studies of Silicon Electrodes for Lithium Ion Batteries: Understanding the (De)lithiation Mechanisms. *J. Am. Chem. Soc.* **2011**, *133*, 503–512.
10. Wu, H.; Cui, Y. Designing Nanostructured Si Anodes for High Energy Lithium Ion Batteries. *Nano Today* **2012**, *7*, 414–429.
11. Cui, L. F.; Ruffo, R.; Chan, C. K.; Peng, H. L.; Cui, Y. Crystalline-Amorphous Core-Shell Silicon Nanowires for High Capacity and High Current Battery Electrodes. *Nano Lett.* **2009**, *9*, 491–495.
12. Johari, P.; Qi, Y.; Shenoy, V. B. The Mixing Mechanism During Lithiation of Si Negative Electrode in Li-Ion Batteries: An Ab Initio Molecular Dynamics Study. *Nano Lett.* **2011**, *11*, 5494–5500.
13. Gu, M.; Li, Y.; Li, X. L.; Hu, S. Y.; Zhang, X. W.; Xu, W.; Thevuthasan, S.; Baer, D. R.; Zhang, J. G.; Liu, J.; *et al. In Situ* TEM Study of Lithiation Behavior of Silicon Nanoparticles Attached to and Embedded in a Carbon Matrix. *ACS Nano* **2012**, *6*, 8439–8447.
14. McDowell, M. T.; Ryu, I.; Lee, S. W.; Wang, C. M.; Nix, W. D.; Cui, Y. Studying the Kinetics of Crystalline Silicon Nanoparticle Lithiation with *In Situ* Transmission Electron Microscopy. *Adv. Mater.* **2012**, *24*, 6034–6041.
15. Liu, X. H.; Zheng, H.; Zhong, L.; Huan, S.; Karki, K.; Zhang, L. Q.; Liu, Y.; Kushima, A.; Liang, W. T.; Wang, J. W.; *et al.* Anisotropic Swelling and Fracture of Silicon Nanowires During Lithiation. *Nano Lett.* **2011**, *11*, 3312–3318.
16. Yang, H.; Huang, S.; Huang, X.; Fan, F. F.; Liang, W. T.; Liu, X. H.; Chen, L. Q.; Huang, J. Y.; Li, J.; Zhu, T.; *et al.* Orientation-Dependent Interfacial Mobility Governs the Anisotropic Swelling in Lithiated Silicon Nanowires. *Nano Lett.* **2012**, *12*, 1953–1958.
17. Liu, X. H.; Wang, J. W.; Huang, S.; Fan, F. F.; Huang, X.; Liu, Y.; Krylyuk, S.; Yoo, J.; Dayeh, S. A.; Davydov, A. V.; *et al. In Situ* Atomic-Scale Imaging of Electrochemical Lithiation in Silicon. *Nat. Nanotechnol.* **2012**, *7*, 749–756.
18. Lee, S. W.; McDowell, M. T.; Choi, J. W.; Cui, Y. Anomalous Shape Changes of Silicon Nanopillars by Electrochemical Lithiation. *Nano Lett.* **2011**, *11*, 3034–3039.
19. Liu, X. H.; Fan, F. F.; Yang, H.; Zhang, S. L.; Huang, J. Y.; Zhu, T. Self-Limiting Lithiation in Silicon Nanowires. *ACS Nano* **2013**, *7*, 1495–1503.
20. Cui, L. F.; Yang, Y.; Hsu, C. M.; Cui, Y. Carbon-Silicon Core-Shell Nanowires as High Capacity Electrode for Lithium Ion Batteries. *Nano Lett.* **2009**, *9*, 3370–3374.
21. He, Y.; Yu, X. Q.; Wang, Y. H.; Li, H.; Huang, X. J. Alumina-Coated Patterned Amorphous Silicon as the Anode for a Lithium-Ion Battery with High Coulombic Efficiency. *Adv. Mater.* **2011**, *23*, 4938–4941.
22. McDowell, M. T.; Lee, S. W.; Ryu, I.; Wu, H.; Nix, W. D.; Choi, J. W.; Cui, Y. Novel Size and Surface Oxide Effects in Silicon Nanowires as Lithium Battery Anodes. *Nano Lett.* **2011**, *11*, 4018–4025.
23. Zhao, K. J.; Wang, W. L.; Gregoire, J.; Pharr, M.; Suo, Z. G.; Vlassak, J. J.; Kaxiras, E. Lithium-Assisted Plastic Deformation of Silicon Electrodes in Lithium-Ion Batteries: A First-Principles Theoretical Study. *Nano Lett.* **2011**, *11*, 2962–2967.
24. Wang, L. F.; Tian, X. Z.; Yang, S. Z.; Xu, Z.; Wang, W. L.; Bai, X. D. Dynamic Nanomechanics of Zinc Oxide Nanowires. *Appl. Phys. Lett.* **2012**, *100*, 163110.
25. Wang, L. F.; Xu, Z.; Yang, J. L.; Tian, X. Z.; Wei, J. K.; Wang, W. L.; Bai, X. D. Real Time *in Situ* TEM Studying the Fading Mechanism of Tin Dioxide Nanowire Electrodes in Lithium Ion Batteries. *Science China Technological Sciences* **2013**, *56*, 2630–2635.
26. Gao, P.; Kang, Z. C.; Fu, W. Y.; Wang, W. L.; Bai, X. D.; Wang, E. G. Electrically Driven Redox Process in Cerium Oxides. *J. Am. Chem. Soc.* **2010**, *132*, 4197–4201.
27. Wang, L. F.; Xu, Z.; Wang, W. L.; Bai, X. D. Atomic Mechanism of Dynamic Electrochemical Lithiation Processes of MoS_2 Nanosheets. *J. Am. Chem. Soc.* **2014**, *136*, 6693–6697.
28. Li, H.; Huang, X. J.; Chen, L. Q.; Zhou, G. W.; Zhang, Z.; Yu, D. P.; Mo, Y. J.; Pei, N. The Crystal Structural Evolution of Nano-Si Anode Caused by Lithium Insertion and Extraction at Room Temperature. *Solid State Ionics* **2000**, *135*, 181–191.
29. Key, B.; Bhattacharyya, R.; Morcrette, M.; Seznec, V.; Tarascon, J. M.; Grey, C. P. Real-Time NMR Investigations of Structural Changes in Silicon Electrodes for Lithium-Ion Batteries. *J. Am. Chem. Soc.* **2009**, *131*, 9239–9249.
30. McDowell, M. T.; Lee, S. W.; Harris, J. T.; Korgel, B. A.; Wang, C. M.; Nix, W. D.; Cui, Y. *In Situ* TEM of Two-Phase Lithiation of Amorphous Silicon Nanospheres. *Nano Lett.* **2013**, *13*, 758–764.
31. Wang, J. W.; He, Y.; Fan, F. F.; Liu, X. H.; Xia, S. M.; Liu, Y.; Harris, C. T.; Li, H.; Huang, J. Y.; Mao, S. X.; *et al.* Two-Phase Electrochemical Lithiation in Amorphous Silicon. *Nano Lett.* **2013**, *13*, 709–715.
32. Liu, X. H.; Zhong, L.; Huang, S.; Mao, S. X.; Zhu, T.; Huang, J. Y. Size-Dependent Fracture of Silicon Nanoparticles During Lithiation. *ACS Nano* **2012**, *6*, 1522–1531.
33. Sethuraman, V. A.; Chon, M. J.; Shimshak, M.; Van Winkle, N.; Guduru, P. R. *In Situ* Measurement of Biaxial Modulus of Si Anode for Li-Ion Batteries. *Electrochem. Commun.* **2010**, *12*, 1614–1617.
34. Goldman, J. L.; Long, B. R.; Gewirth, A. A.; Nuzzo, R. G. Strain Anisotropies and Self-Limiting Capacities in Single-Crystalline 3D Silicon Microstructures: Models for High Energy Density Lithium-Ion Battery Anodes. *Adv. Funct. Mater.* **2011**, *21*, 2412–2422.
35. McDowell, M. T.; Lee, S. W.; Nix, W. D.; Cui, Y. 25th Anniversary Article: Understanding the Lithiation of Silicon and other Alloying Anodes for Lithium-Ion Batteries. *Adv. Mater.* **2013**, *25*, 4966–4984.
36. Lee, S. W.; McDowell, M. T.; Berla, L. A.; Nix, W. D.; Cui, Y. Fracture of Crystalline Silicon Nanopillars During Electrochemical Lithium Insertion. *Proc. Natl. Acad. Sci. U.S.A.* **2012**, *109*, 4080–4085.
37. Dresselhaus, M. S.; Dresselhaus, G. Intercalation Compounds of Graphite. *Adv. Phys.* **2002**, *51*, 1–186.